Plasmon resonant amplification of hot electron-driven photocatalysis

Lang Shen, George N. Gibson, Nirakar Poudel, Bingya Hou, Jihan Chen, Haotian Shi, Ernest Guignon, Nathaniel C. Cady, William D. Page, Arturo Pilar, and Stephen B. Cronin

Citation: Appl. Phys. Lett. **113**, 113104 (2018); doi: 10.1063/1.5048582
View online: https://doi.org/10.1063/1.5048582
View Table of Contents: http://aip.scitation.org/toc/apl/113/11
Published by the American Institute of Physics

Plasmon resonant amplification of hot electron-driven photocatalysis

Lang Shen,[1] George N. Gibson,[2,3] Nirakar Poudel,[4] Bingya Hou,[4] Jihan Chen,[4] Haotian Shi,[5] Ernest Guignon,[3] Nathaniel C. Cady,[6] William D. Page,[3] Arturo Pilar,[3] and Stephen B. Cronin[4,5,7,a)]

[1]*Mork Family Department of Chemical Engineering and Materials Science, University of Southern California, Los Angeles, California 90089, USA*
[2]*Department of Physics, University of Connecticut, Storrs, Connecticut 06269, USA*
[3]*Ciencia Inc., East Hartford, Connecticut 06108, USA*
[4]*Ming Hsieh Department of Electrical Engineering, University of Southern California, Los Angeles, California 90089, USA*
[5]*Department of Chemistry, University of Southern California, Los Angeles, California 90089, USA*
[6]*Colleges of Nanoscale Science and Engineering, SUNY Polytechnic Institute, Albany, New York 12203, USA*
[7]*Department of Physics and Astronomy, University of Southern California, Los Angeles, California 90089, USA*

(Received 16 July 2018; accepted 27 August 2018; published online 11 September 2018)

We report plasmon resonant excitation of hot electrons in a metal based photocatalyst in the oxygen evolution half reaction in aqueous solution. Here, the photocatalyst consists of a 100-nm thick Au film deposited on a corrugated silicon substrate. In this configuration, hot electrons photoexcited in the metal are injected into the solution, ultimately reversing the water oxidation reaction ($O_2 + 4H^+ + 4e^- \leftrightharpoons 2H_2O$) and producing a photocurrent. In order to amplify this process, the gold electrode is patterned into a plasmon resonant grating structure with a pitch of 500 nm. The photocurrent (i.e., charge transfer rate) is measured as a function of incident angle using 633 nm wavelength light. We observe peaks in the photocurrent at incident angles of $\pm 9°$ from normal when the light is polarized parallel to the incident plane (p-polarization) and perpendicular to the lines on the grating. Based on these peaks, we estimate an overall plasmonic gain (or amplification) factor of $2.1\times$ in the charge transfer rate. At these same angles, we also observe sharp dips in the photoreflectance, corresponding to the condition when there is wavevector matching between the incident light and the plasmon mode in the grating. No angle dependence is observed in the photocurrent or photoreflectance when the incident light is polarized perpendicular to the incident plane (s-polarization) and parallel to the lines on the grating. Finite difference time domain simulations also predict sharp dips in the photoreflectance at $\pm 9°$, and the electric field intensity profiles show clear excitation of a plasmon-resonant mode when illuminated at those angles with p-polarized light. *Published by AIP Publishing.* https://doi.org/10.1063/1.5048582

Plasmon-enhanced photocatalytic water splitting was first reported in 2011 and was attributed to the enhanced local electrical field produced by the plasmon resonance phenomenon, which increases the light absorption in a semiconductor material TiO_2 with the existence of sub-bandgap states (i.e., defect states).[1–3] More recently, however, more attention has been drawn to a completely different mechanism, involving hot electron injection (HEI), which further exploits plasmon enhancement in photocatalytic reactions. Here, the basic concept is that hot electrons can be generated through the decay of plasmons, and these high energy electrons can then directly participate in and facilitate desired chemical reactions, acting as a novel photocatalyst. Using hot electrons in metals to drive photocatalytic processes was first put forth by Mukherjee, who reported photodissociation of H_2 on Au nanoparticles deposited on SiO_2 and TiO_2 supports.[4,5] The dissociation of H_2 and D_2 using plasmons was probed by post-reaction detection of HD formation. Their work provides key insights into HEI but more extended studies are needed in order to apply the concept of HEI to a broader set of applications and reaction systems. Both the Brongersma and Halas groups have reported hot electron processes in solid state devices enhanced by plasmonic grating structures.[6,7] While their works present further evidence of HEI in metal/oxide/metal structures, adopting this general idea to photocatalysis requires further development and experimentations. DuChene reported the use of hot electrons in a plasmonic-metal/semiconductor heterostructure for photocatalytic water splitting.[8] In their work, TiO_2 nanowire arrays were used in combination with Au nanoparticles to enhance anodic photocurrents via HEI under periodic visible-light irradiation. In the work of Robatjazi, plasmon resonant nanoparticles were deposited on the top of NiO_x semiconducting films, and the resulting photocurrent generated was attributed to HEI to ions in the solution.[9] However, in these previous sample configurations, in which semiconductor materials surrounded the plasmonic structures, it was difficult to isolate the role of HEI in the photocatalytic enhancement and separate the enhanced photoresponse from enhanced local fields. In a more direct observation, Hou measured photocatalytic water splitting on a bare Au film without any semiconducting material present.[10] Here, an AC lock-in technique was used to detect the relatively small photocurrents produced by the short-lived hot electrons in the

a)Author to whom correspondence should be addressed: scronin@usc.edu

bulk metal film (∼10 fs). The photocurrents from these bulk metal photoanodes were attributed to photo-generated hot electrons in the Au film. In addition, there have been several recent theoretical studies concluding that plasmon resonant excitations decay into hot electrons in metal nanostructures,[11–16] which opens up the exciting possibility of amplifying the relatively small photocurrents (i.e., charge transfer rates and efficiencies) using plasmon resonant nanostructures.[17–24]

In this work, we utilize plasmonic grating structures as a platform to study and isolate the effect of plasmon resonant excitations on hot electron-driven photocatalysis. These plasmonic nanostructures consist only of Au, thus, ruling out any complications associated with semiconductor materials and/or sub-bandgap absorption. Here, we study the effect of hot electrons on the canonical photoelectrochemical reaction system of water splitting. Experimentally, these gratings enable us to easily tune between resonant and non-resonant excitation by switching the polarization of the incident light between p-polarization and s-polarization without changing any other variables (e.g., wavelength, intensity, or material composition). Using this approach, we can distinguish the photoresponse associated with plasmon resonant excitations and bulk metal absorption. The resonance conditions for the plasmon mode can be verified by sweeping the incident angle of p-polarized light and comparing the angle dependence of photoreflectance and photocurrent. Further details regarding the nature of the plasmon resonance are obtained from electromagnetic simulations based on these grating nanostructures using the finite difference time domain method (FDTD, Lumerical).

Metal gratings used in this work consist of a 100 nm gold film with a 10 nm Ti adhesion layer deposited on the top of a corrugated Si wafer with a pitch of 500 nm and a grating area of $1 \times 1\,\mathrm{cm}^2$. These grating structures were fabricated using the same method as reported by Rice.[25] Figure 1(a) shows the cross-sectional image of the grating obtained by using scanning electron microscopy (SEM). Figure 1(b) shows an illustration of the sample geometry, where electrical connection was made directly to the top Au surface, thus keeping the bottom Si substrate out of the circuit in all the electrochemical measurements. Copper wires with an insulating coating and silver paint (SPI Supplies, Inc.) were used to electrical contact, and 5-min epoxy was used to encapsulate the sample. The sample was mounted on a rotational stage and illuminated with collimated light, as shown in Fig. 2(a). Figure 2(b) shows the photoelectrochemical measurement setup with a three-terminal configuration. The grating sample was measured as the working electrode, and a Ag/AgCl electrode and a Pt wire (BASi, Corp.) were used as the reference and counter electrodes, respectively. The measurements were conducted in a 0.5 M Na_2SO_4 (Anhydrous ACS, VWR) solution, and the potential of the working electrode was varied using a Gamry potentiostat (Gamry, Inc.). To detect small photocurrents around a few micro-amperes, we used an AC lock-in technique similar to those reported previously.[10,26] Here, an optical chopper (SR540, Stanford Research Systems, Inc.) was used in combination with a lock-in amplifier (SRS830, Stanford Research Systems, Inc.). The optical chopper is used to modulate the incident laser (633 nm HeNe laser, maximum power 35 mW, and beam diameter 0.3 cm^2) at a frequency of

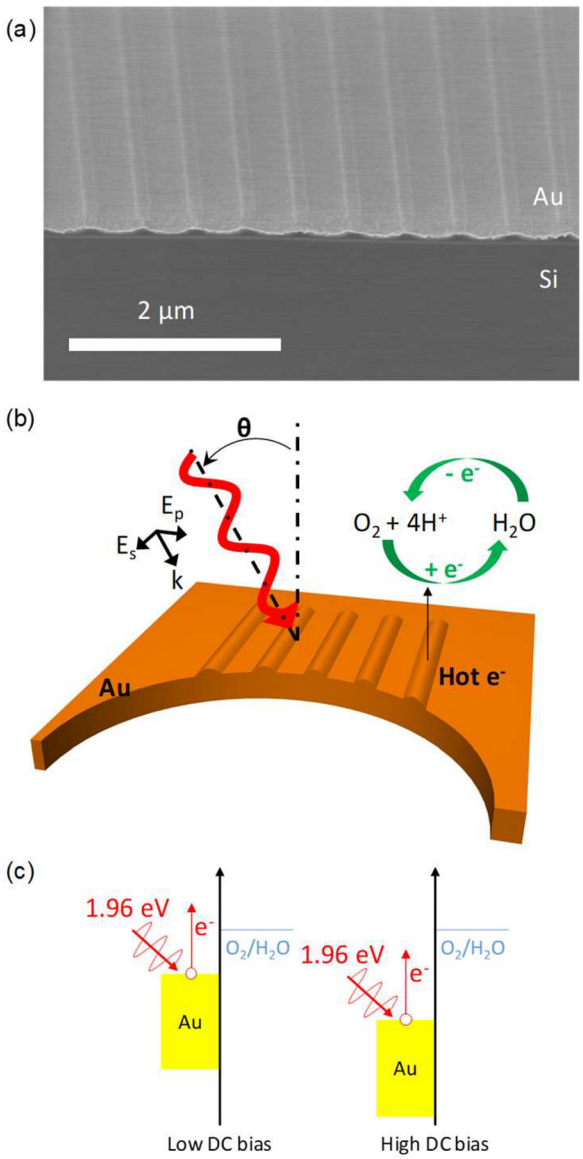

FIG. 1. (a) Cross-sectional scanning electron microscope (SEM) image and (b) schematic diagram of the plasmon resonant grating structure. (c) Illustration of the hot electron injection mechanism.

4–400 Hz. Any photoresponse produced in the working electrode will generate an AC component in the current output at the same frequency of the chopper, which can then be detected and measured by the lock-in amplifier.

The photoresponse of the plasmonic gratings plotted as a function of the incident angle is shown in Fig. 2(c). When the incident light is s-polarized (i.e., parallel to the grating lines and perpendicular to the incident plane), an angle-independent photocurrent is observed. The finite current observed under s-polarized light is possibly due to surface roughness. A clear angle-dependent photocurrent is observed under p-polarized light (perpendicular to the grating lines and parallel to the incident plane). Due to the symmetry of our grating structures, two symmetric maxima in the photocurrent under p-polarization can be seen at ±9° from normal incidence. By comparing the photocurrent at ±9° for the two polarizations, we estimate an amplification factor of 210% for hot electron generation in the metal grating by exploiting the plasmon resonance conditions. Here, we estimate the

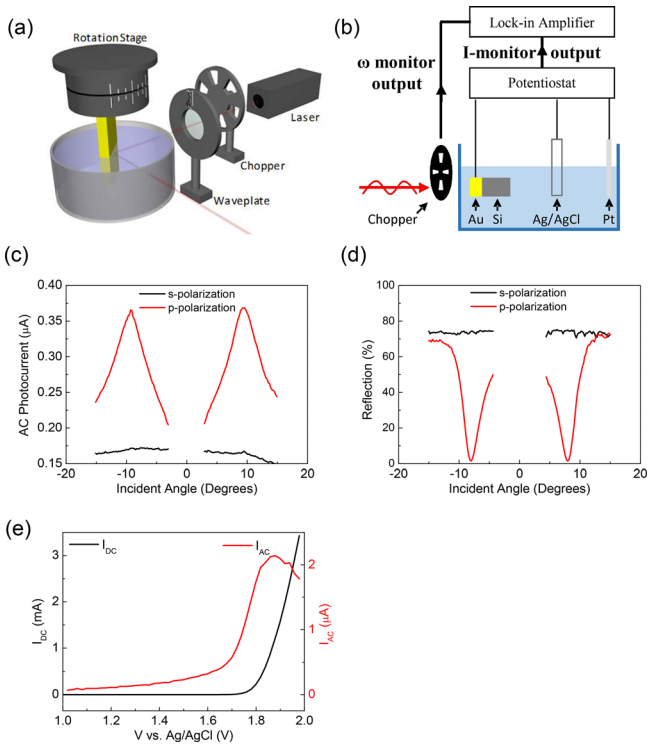

FIG. 2. (a) and (b) Schematic diagrams of the experimental measurement configuration. (c) AC photocurrent and (d) photoreflectance plotted as a function of the incident angle for 633 nm light with an intensity of 106 mW/cm^2 polarized parallel and perpendicular to the grating structure. (e) DC current and AC photocurrent plotted as a function of reference potential when illuminated at 9° with respect to normal incidence.

"noise" in our data to be approximately 10 nA. The maximum signal observed on resonance is 350 nA, which corresponds to an error in the enhancement factor of 210% ± 3%. We estimate the quantum efficiency, here, to be on the order of 0.007% electrons per incident photon under resonant conditions. The primary focus of this work is to demonstrate the existence of hot electrons in our plasmonic grating system and to study HEI as a catalytic mechanism in photoelectrochemical water splitting without the interference of semiconductor materials. In the proof-of-principle work reported here, we have only explored a fixed wavelength (633 nm) with a pre-designed grating structure. As such, the overall efficiency of the system is likely to be far from optimum. Further optimization of the system and improvement of the overall efficiency of water splitting will be explored in our future studies. Typically, grating structures can couple up to 40% of the far field energy into the confined field of the propagating surface plasmon, depending strongly also on the wavelength and groove density.[27] We anticipate that this represents a hard upper limit on potential performance of these grating-based photocatalytic devices. The photoreflectance of the grating after Au deposition was also measured in the same solution used for the photocurrent measurements. The dip at ±9° from normal incidence is a clear signature of wavevector matching between the incident light and the plasmon resonant mode of the grating. Figure 2(e) shows the DC and AC currents plotted as a function of reference potential, which exhibits a clear onset of the AC photocurrent around 1.5 V and a maximum around 1.88 V versus the reference electrode (Ag/AgCl). Here, it is important to note that the DC bias supplied by the potentiostat is driving a water oxidation reaction (i.e., $2H_2O \leftrightharpoons O_2 + 4H^+ + 4e^-$), which is observed in the form of a DC current. In this DC bias range, the photoexcited hot electrons near the top surface of the Au electrode can be injected into the solution and reduce the products and intermediates generated in the oxidation reaction, resulting in a reverse reaction and corresponding photocurrent [I_{AC} is represented as the red line in Fig. 2(e)]. Here, I_{AC} is directly related to the rate at which hot electrons are consumed in the reverse reaction. At lower biases, the reaction rate is limited by the amount of products (and intermediates) that are supplied from DC water oxidation. As such, I_{AC} begins small at low applied potentials and increases as the potential increases, which drives more water oxidation. At higher potentials (1.8 V), the Fermi energy of Au is lowered to a position well below the redox couple potential, thus shutting off the reaction and quenching the AC photocurrent, as shown in Fig. 1(c).

To provide a more detailed picture of the plasmon resonance in these gratings, we performed electromagnetic simulations using the FDTD method. The grating structure used in these FDTD simulations (i.e., an infinite Si substrate with a 500 nm-pitch corrugated surface and 100 nm-thick Au) was imported from the cross-sectional SEM image (see Fig S2 for the cross-section profile plot), and all simulations were performed using a background refractive index of 1.3317 (for H_2O at 633 nm). A mesh size of 0.1 nm and periodic boundaries for x and z directions and perfectly matched layer (PML) boundaries for the y direction were used for the simulated region. A plane wave source with different incident angles and polarization directions was used as the excitation source, and a plane power monitor in the y-plane was used to capture all the reflected light from the grating surface. Power monitors in the z-plane were placed to obtain the electrical field profiles for different irradiation conditions. The calculated reflectance for both polarizations is plotted in Fig. 3(a). The simulated data for both polarizations reproduce the behavior observed in our experimental measurements with the p-polarized light producing sharp dips in the reflectance at ±9° and s-polarization showing no angle dependence and nearly constant reflection. The electric field intensity distributions are plotted in Figs. 3(b) and 3(c) for p-polarization and Figs. 3(d) and 3(e) for s-polarization. When the incident light is not coupled to the plasmon modes [Figs. 3(b), 3(d), and 3(e)], low electric field intensities (i.e., non-resonant behavior) are observed for all three cases. With p-polarized light at 9° incidence, we can observe clear excitation of the plasmon resonance. The ratio of the electric field intensity of the brightest point on the metal surface is 21.3× larger under p-polarized than under s-polarized illumination (i.e., $|E_p|^2/|E_s|^2 = 21.3$). However, in order to more accurately predict the enhancement factor observed experimentally, we must integrate over the metal surface. Based on these simulations, we can calculate the relative density of hot electrons by integrating the electric field intensity in the metal ($|E|^2$), which is proportional to the hot electron generation rate, under both s- and p-polarization conditions. In the z-dimension, we integrate from the top metal surface [$z = f(x,y)$] to one mean free path length below the surface [$z = f(x,y) - \lambda_{Au}$], as described in the following equation:[28]

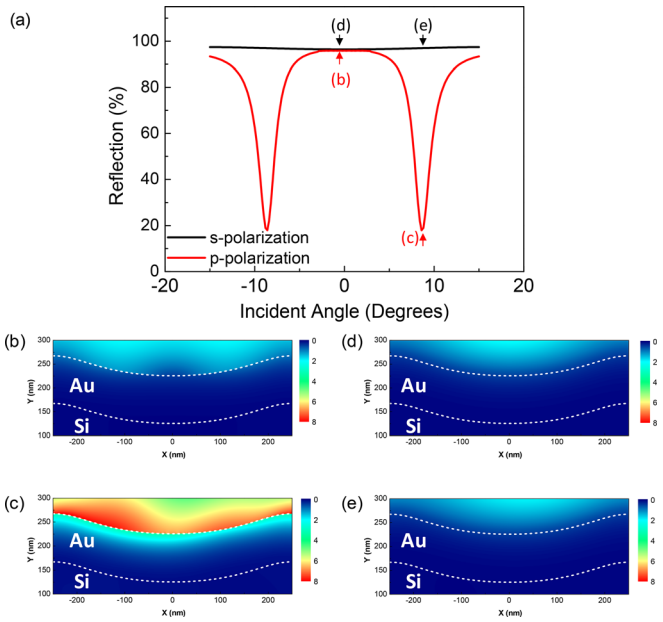

FIG. 3. (a) Finite difference time domain (FDTD) simulations of the photoreflectance as a function of the incident angle for p- and s-polarized 633 nm light. Cross-sectional electric field intensity profiles for illumination at (b) p-polarized and normal incidence, (c) p-polarized and 9° incidence, (d) s-polarized and normal incidence, and (e) s-polarized and 9° incidence.

$$EF = \frac{\int_{f(x,y)-20\,\mathrm{nm}}^{f(x,y)} |E_p|^2 dxdydz}{\int_{f(x,y)-20\,\mathrm{nm}}^{f(x,y)} |E_s|^2 dxdydz}. \quad (1)$$

Based on literature values of the mean free path of electrons with different energies above the Fermi level, we use 20 nm for electrons with 1.96 eV energy for our estimation here.[29] Performing this integral yields an average integrated enhancement of 15.9×. While the results of our FDTD simulations agree well with our experimental data [see Figs. 2(b) and 3(a)], the experimental enhancement factor is considerably lower than these simulations. This discrepancy reflects the fact that losses occur as the hot electrons are transferred to the ions in the solution, which are not taken into account the electromagnetic simulations. The simulation results show that the maximum number of photons can be absorbed by tuning to plasmon resonance, indicating the theoretical limit of the enhancement factor in our system.

As a final check, Fig. S1 of the supplementary material shows a comparison of the diffuse reflectance spectra of the plasmon resonant grating structure and a bare Au film. Here, we observe a sharp resonance centered around 630 nm for the grating structure while the spectrum of the bare Au film is featureless. This data further demonstrate that the phenomenon we are observing here is plasmonic in nature.

In conclusion, plasmon resonant excitation of hot electrons is observed in a metal based photocatalyst, which is used to drive the reverse reaction of water oxidation. In this configuration, hot electrons, photoexcited in the metal, inject into the aqueous solution and reverse the water oxidation half reaction ($O_2 + 4H^+ + 4e^- \leftrightharpoons H_2O$), thus producing a photocurrent. By utilizing a plasmonic grating structure under resonant conditions, we demonstrate amplification of this process. The photocurrent and hence the charge transfer rate are measured with respect to the angle of incidence with 633 nm wavelength light. Sharp peaks in the photocurrent are observed at incident angles of ±9° when the light is polarized perpendicular to the grating (p-polarization). We also observe sharp dips in the photoreflectance with similar angle dependence, which correspond to the condition when there is good wavevector matching between the incident light and the plasmon mode in the grating. When illuminated with light polarized parallel to the grating (s-polarization), we observe no angle dependence in the photocurrent or photoreflectance. Based on these data, we estimate a plasmonic gain factor of 2.1× in the charge transfer rate when irradiated under resonant conditions. Electromagnetic (FDTD) simulations corroborate the sharp dips observed in the photoreflectance at ±9° and provide a detailed picture of the electric field intensity profiles, which show the excitation of a plasmon resonant mode, when illuminated under resonant conditions (i.e., 9° and p-polarization).

See supplementary material for diffuse reflectance spectra of Au grating, cross-section profile of grating, and photocurrent of an Au film on a glass slide.

This research was supported by NSF Award No. CBET-1512505 (L.S.), Air Force Office of Scientific Research Grant No. FA9550-15-1-0184 (B.H.), ARO Award No. W911NF-14–1-0228 (H.S.), Department of Energy (DOE) Award No. DE-FG02-07ER46376 (N.P.), and ACS-PRF Grant No. 55993-ND5 (J.C.).

[1]D. B. Ingram and S. Linic, "Water splitting on composite plasmonic-metal/semiconductor photoelectrodes: Evidence for selective plasmon-induced formation of charge carriers near the semiconductor surface," J. Am. Chem. Soc. **133**(14), 5202–5205 (2011).
[2]C. G. Silva, R. Juarez, T. Marino, R. Molinari, and H. Garcia, "Influence of excitation wavelength (UV or visible light) on the photocatalytic activity of titania containing gold nanoparticles for the generation of hydrogen or oxygen from water," J. Am. Chem. Soc. **133**(3), 595–602 (2011).
[3]Z. Liu, W. Hou, P. Pavaskar, M. Aykol, and S. B. Cronin, "Plasmon resonant enhancement of photocatalytic water splitting under visible illumination," Nano Lett. **11**(3), 1111–1116 (2011).
[4]S. Mukherjee, F. Libisch, N. Large, O. Neumann, L. V. Brown, J. Cheng, J. B. Lassiter, E. A. Carter, P. Nordlander, and N. J. Halas, "Hot electrons do the impossible: Plasmon-induced dissociation of H_2 on Au," Nano Lett. **13**(1), 240–247 (2013).
[5]S. Mukherjee, L. Zhou, A. M. Goodman, N. Large, C. Ayala-Orozco, Y. Zhang, P. Nordlander, and N. J. Halas, "Hot-electron-induced dissociation of H_2 on gold nanoparticles supported on SiO_2," J. Am. Chem. Soc. **136**(1), 64–67 (2014).
[6]H. Chalabi, D. Schoen, and M. L. Brongersma, "Hot-electron photodetection with a plasmonic nanostripe antenna," Nano Lett. **14**(3), 1374–1380 (2014).
[7]B. Y. Zheng, H. Zhao, A. Manjavacas, M. McClain, P. Nordlander, and N. J. Halas, "Distinguishing between plasmon-induced and photoexcited carriers in a device geometry," Nat. Commun. **6**, 7797 (2015).
[8]J. S. DuChene, B. C. Sweeny, A. C. Johnston-Peck, D. Su, E. A. Stach, and W. D. Wei, "Prolonged hot electron dynamics in plasmonic-metal/semiconductor heterostructures with implications for solar photocatalysis," Angew. Chem. **53**(30), 7887–7891 (2014).
[9]H. Robatjazi, S. M. Bahauddin, C. Doiron, and I. Thomann, "Direct plasmon-driven photoelectrocatalysis," Nano Lett. **15**(9), 6155–6161 (2015).
[10]B. Hou, L. Shen, H. Shi, R. Kapadia, and S. B. Cronin, "Hot electron-driven photocatalytic water splitting," Phys. Chem. Chem. Phys. **19**, 2877 (2017).

[11]A. O. Govorov, H. Zhang, and Y. K. Gun'ko, "Theory of photoinjection of hot plasmonic carriers from metal nanostructures into semiconductors and surface molecules," J. Phys. Chem. C **117**(32), 16616–16631 (2013).
[12]T. Tatsuma, H. Nishi, and T. Ishida, "Plasmon-induced charge separation: Chemistry and wide applications," Chem. Sci. **8**(5), 3325–3337 (2017).
[13]R. Sundararaman, P. Narang, A. S. Jermyn, W. A. Goddard III, and Atwater, H. A., "Theoretical predictions for hot-carrier generation from surface plasmon decay," Nat. Commun. **5**, 5788 (2014).
[14]A. M. Brown, R. Sundararaman, P. Narang, W. A. Goddard III, and H. A. Atwater, "Nonradiative plasmon decay and hot carrier dynamics: Effects of phonons, surfaces, and geometry," ACS Nano **10**(1), 957–966 (2016).
[15]P. Narang, R. Sundararaman, and H. A. Atwater, "Plasmonic hot carrier dynamics in solid-state and chemical systems for energy conversion," Nanophotonics **5**(1), 96–111 (2016).
[16]H. Sakurai and M. Haruta, "Synergism in methanol synthesis from carbon dioxide over gold catalysts supported on metal oxides," Catal. Today **29**(1-4), 361–365 (1996).
[17]M. L. Brongersma, N. J. Halas, and P. Nordlander, "Plasmon-induced hot carrier science and technology," Nat. Nanotechnol. **10**(1), 25–34 (2015).
[18]C. Clavero, "Plasmon-induced hot-electron generation at nanoparticle/metal-oxide interfaces for photovoltaic and photocatalytic devices," Nat. Photonics **8**(2), 95–103 (2014).
[19]C. Kim, B. L. Suh, H. Yun, J. Kim, and H. Lee, "Surface plasmon aided ethanol dehydrogenation using Ag-Ni binary nanoparticles," ACS Catal. **7**(4), 2294–2302 (2017).
[20]A. Naldoni, T. Montini, F. Malara, M. M. Mroz, A. Beltram, T. Virgili, C. L. Boldrini, M. Marelli, I. Romero-Ocana, J. J. Delgado, V. Dal Santo, and P. Fornasiero, "Hot electron collection on brookite nanorods lateral facets for plasmon-enhanced water oxidation," ACS Catal. **7**(2), 1270–1278 (2017).
[21]W. Y. Lei, T. T. Zhang, P. Liu, J. A. Rodriguez, G. Liu, and M. H. Liu, "Bandgap- and local field-dependent photoactivity of Ag/black phosphorus nanohybrids," ACS Catal. **6**(12), 8009–8020 (2016).
[22]B. H. Wu, W. T. Liu, T. Y. Chen, T. P. Perng, J. H. Huang, and L. J. Chen, "Plasmon-enhanced photocatalytic hydrogen production on Au/TiO_2 hybrid nanocrystal arrays," Nano Energy **27**, 412–419 (2016).
[23]S. M. Kim, S. W. Lee, S. Y. Moon, and J. Y. Park, "The effect of hot electrons and surface plasmons on heterogeneous catalysis," J. Phys.-Condens. Matter **28**(25), 254002 (2016).
[24]S. Linic, P. Christopher, and D. B. Ingram, "Plasmonic-metal nanostructures for efficient conversion of solar to chemical energy," Nat. Mater. **10**(12), 911–921 (2011).
[25]J. M. Rice, L. J. Stern, E. F. Guignon, D. A. Lawrence, and M. A. Lynes, "Antigen-specific T cell phenotyping microarrays using grating coupled surface plasmon resonance imaging and surface plasmon coupled emission," Biosens. Bioelectron. **31**(1), 264–269 (2012).
[26]J. B. Sambur, S. C. Riha, D. Choi, and B. A. Parkinson, "Influence of surface chemistry on the binding and electronic coupling of CdSe quantum dots to single crystal TiO_2 surfaces," Langmuir **26**(7), 4839–4847 (2010).
[27]A. Giugni, B. Torre, M. Allione, G. Das, Z. W. Wang, X. He, H. N. Alshareef, and E. Di Fabrizio, "Experimental route to scanning probe hot-electron nanoscopy (HENs) applied to 2D material," Adv. Opt. Mater. **5**(15), 1700195 (2017).
[28]D. Gall, "Electron mean free path in elemental metals," J. Appl. Phys. **119**(8), 085101 (2016).
[29]S. M. Sze, J. L. Moll, and T. Sugano, "Range-energy relation of hot electrons in gold," Solid State Electron. **7**(7), 509–523 (1964).